IEEE Access
Multidisciplinary | Rapid Review | Open Access Journal

Received December 1, 2017, accepted January 5, 2018, date of publication January 12, 2018, date of current version May 16, 2018.

Digital Object Identifier 10.1109/ACCESS.2018.2792448

Permeance Analysis and Calculation of the Double-Radial Rare-Earth Permanent Magnet Voltage-Stabilizing Generation Device

XUEYI ZHANG[1], QINJUN DU[2], SHILUN MA[1], HUIHUI GENG[1], WENJING HU[1], ZHIWU LI[3], (Fellow, IEEE), AND GUOQIANG LIU[1]

[1]School of Transportation and Vehicle Engineering, Shandong University of Technology, Zibo 255049, China
[2]School of Electrical and Electronic Engineering, Shandong University of Technology, Zibo 255049, China
[3]Institute of Systems Engineering, Macau University of Science and Technology, Macau 999078, China

Corresponding author: Xueyi Zhang (zhangxueyi@sdut.edu.cn)

This work was supported in part by the National Natural Science Foundation of China under Grant 51507096 and in part by the Shandong Province Natural Science Foundation of China under Grant ZR2018LE010.

ABSTRACT The structure and magnetic circuit of the modern permanent magnet (PM) generator are often very complicated, which makes the traditional finite element analysis of magnetic field highly difficult. This paper establishes an equivalent magnetic circuit model of a new double-radial PM generator using the traditional equivalent circuit method and data analysis, introduces the calculation formulas of permeance and leakage permeance (LP) in magnetic circuits in detail, analyzes the influence factors of the LP, and provides the solutions. These studies will have a certain guiding significance for the design and optimization of generator circuits. To obtain the best matching parameters, the main parameters of the generator are tested and analyzed, such as the thickness of PM steel in the magnetization direction, length of PM steel, number of pole pairs, and the thickness of spacer bush. Finally, a prototype is tested, and the results show that the output characteristics of the designed double-radial PM voltage-stabilizing generation device are very good.

INDEX TERMS Data analysis, double-radial rare-earth permanent magnet, equivalent magnetic circuit model, permeance analysis, vehicles, voltage-stabilizing generation device.

I. INTRODUCTION

Silicon rectifier generators, which are used in vehicles, often use electric field winding to produce magnetic fields. However, only a little part of the energy can be converted into magnetic energy for electricity generation; most of the electrical energy is dissipated as heat from the electric field winding [1], [2]. In contrast, the permanent magnet (PM) generator has low heat loss because PM steel was used instead of excitation winding, and it has the advantages of high efficiency and high reliability because of the use of Nd-Fe-B PM material [3]–[6]. Therefore, many experts and researchers have made many in-depth explorations on PM generators. Saeid Javadi et al. designed and analyzed a 42V coreless axial-flux permanent-magnet generator for automotive applications. This structure is a special design which is suitable for flux weakening at variable speeds. Zhang *et al.* [7] conducted a contrastive study of two types of armature topology of ultra-high-speed PM generator and proposed a reasonable design scheme of armature winding. Nishida *et al.* [8] proposed a small-scale active power filter to regulate the output voltage of the designed variable-speed interior PM synchronous generator by controlling its reactive current component and filtering the harmonic current generated by a non-linear diode rectifier load. A 1.5kW laboratory prototype has been built to confirm the feasibility of the proposed method. Chan *et al.* [9] analyzed the steady-state and transient performance of a surface-inset PM synchronous generator that feeding an isolated load used a coupled-circuit, time-stepping, and 2D finite-element analysis. Cheng *et al.* [10] proposed an analytical model using the d/q-axis model to estimate the maximal output power that corresponded to the current and power angle of a high-speed PM synchronous generator. Qazalbash *et al.* [11] calculated the on-load rotor eddy current power loss of PM machines using finite-element analysis methods, where they considered the eddy current effect. Jang *et al.* [12] analyzed the eddy current loss of a double-sided cored slotless-type PM linear synchronous generator using the space harmonic method. Zhang *et al.* [13] established a 2D transient electromagnetic field mathematical model for super-high-speed PM generators using the circuit-field coupled time-stepping finite-element method, and calculated the temperature

distributions and cooling medium using the 3D finite volume method. The obtained conclusion can provide a guiding significance for the designing of super-high-speed PM generators [14], [15].

By analyzing the existing results, we conclude that prior studies mainly focus on the structure design, output performance, voltage control, and generator loss. But the research on the establishment and analysis of magnetic field model of the generator is simple. However, the structure and magnetic field of modern PM generators are commonly very complicated [16], [17], which causes a very complex process of preprocessing and post-processing finite-element analysis. To obtain more accurate simulation results, the quality of the model subdivision must be very high, which leads to the problem of a long simulation time and low efficiency. The traditional equivalent magnetic circuit method (TEMCM) [18] based on the idea of a ''field circuit'' has the advantages of clear physical meaning, easy realization, and short calculation time, so it is very suitable for the design and prediction of the initial generator scheme. However, the studies using this method commonly only provide the equivalent magnetic circuit model (EMCM), and few people have analyzed each part of the magnetic field model in detail. This study establishes the EMCM of the designed PM generator using the TEMCM method and provides a detailed calculation method for each permeance to evaluate the feasibility of the magnetic field. The work has four contributions: (1) A new double-radial rare-earth PM voltage-stabilizing generation device is proposed, where the air-gap flux of each pair of poles is provided by two adjacent tile-shaped PM steels which are fixed on the rotor yoke and a rectangle PM steel which is embedded in the rectangular groove of the rotor core, so that its air-gap flux density is large and output power is high. (2) The EMCM of the generator is established using the TEMCM, and the calculation method of each permeance is shown in detail, which has a certain guiding significance for the design and optimization of the generator circuit. (3) The generator's 2D model is established using the finite-element software, and the magnetic field is analyzed to verify the rationality of the designed magnetic field. (4) The main structural parameters are optimized to improve the performance of the entire machine, a prototype test is performed and the results show that the designed generation device has a good voltage regulation characteristic.

The remainder of this paper is organized as follows: Section 2 establishes the EMCM and 2D simulation model of the entire generator for the magnetic flux analysis. Section 3 optimizes the structure of the entire machine and verifies the output performance. Finally, Section 4 concludes this work.

II. THE MAGNETIC FLUX ANALYSIS OF DOUBLE-RADIAL PM GENERATOR

The whole structure of the double-radial PM generator is shown in Figure 1, and the geometric constraint condition of the rotor is shown in Figure 2. The double-radial PM rotor

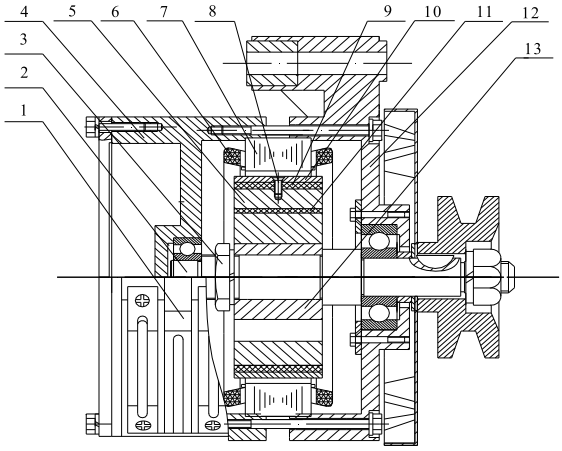

FIGURE 1. Structure diagram of double-radial PM generator. 1. Electronic regulator controller, 2. Axis, 3. Lock nut, 4. Rear cover, 5. Rotor, 6. Armature winding, 7. Stator, 8. Screws, 9. Tile-shaped PM steel, 10. Pole boots, 11. Rectangle PM steel, 12. Front cover, 13. Die-cast aluminum magnetic isolation bushing.

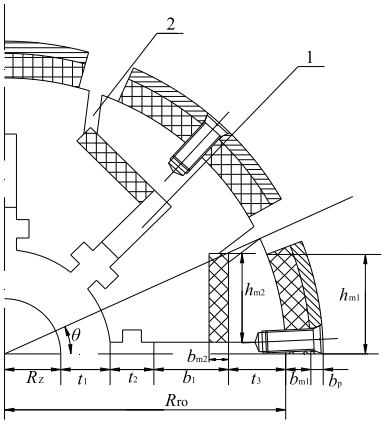

FIGURE 2. Diagram of the rotor geometric constraint. Magnetism isolating air-gap I, 2. Magnetism isolating air-gap II.

is composed of the tile-shaped PM steels which are fixed on the rotor magnetic yoke by non-magnetic screws and the rectangular PM steels which embedded in the rectangular groove of the rotor iron core. These two PM steels provide one air-gap magnetic flux, which can increase the air-gap flux density [19], [20]. The magnetism isolating air-gaps I and II are arranged on the rotor core to avoid magnetic leakage of the PM steels.

A. MAGNETIC CIRCUIT ANALYSIS

On one pair of poles, two adjacent tile-shaped PM steels and one rectangular PM steel are connected in series to provide flux to the air-gap. Based on this, the equivalent magnetic circuit diagram is drawn [21]–[23], as shown in Figure 3.

According to Ohm's law and Kirchhoff's law of magnetic circuits, we can establish the EMCM as follows (1), as shown at the bottom of the next page.

The detailed calculation formula of all parameters are as follows:

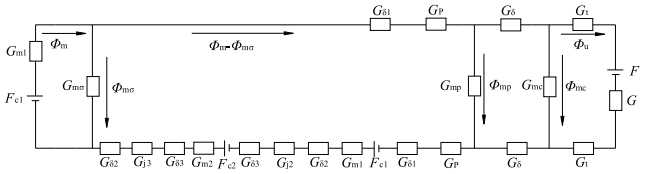

FIGURE 3. Equivalent magnetic circuit diagram of the double-radial PM generator.

1) F_{c1} is the equivalent magnetic potential of tile-shaped PM steel and can be calculated by:

$$F_{c1} = H_c b_{m1} \tag{2}$$

where H_c is the permanent magnetic field intensity and b_{m1} is the thickness of tile-shaped PM steel in the magnetization direction.

2) F_{c2} is the equivalent magnetic potential of rectangle PM steel, and it can be calculated by:

$$F_{c2} = H_c b_{m2} \tag{3}$$

where b_{m2} is the thickness of rectangle PM steel in the magnetization direction.

3) G_{m1} is the equivalent magnetic permeance of tile-shaped PM steel, and it can be calculated by:

$$G_{m1} = \mu_{r1}\mu_0 \frac{S_{m1}}{b_{m1}} \tag{4}$$

where μ_{r1} is the relative permeability of the Nd-Fe-B PM material, and $\mu_{r1} = 1.2$; μ_0 is the permeability of vacuum, and $\mu_0 = 4\pi \times 10^{-7}$H/m; S_{m1} is the surface area of tile-shaped PM steel, and $S_{m1} = 2h_{m1}l_{m1}$, where h_{m1} is the half width of tile-shaped PM steel, and l_{m1} is axial length of tile-shaped PM steel.

4) G_{m2} is the equivalent magnetic permeance of rectangle PM steel, and it can be calculated by:

$$G_{m2} = \mu_{r1}\mu_0 \frac{S_{m2}}{b_{m2}} \tag{5}$$

where S_{m2} is the surface area of rectangle PM steel $S_{m2} = h_{m2}l_{m2}$, where h_{m2} is the width of rectangle PM steel, and l_{m2} is the axial length of rectangular PM steel.

5) $G_{m\sigma}$ is the leakage permeance (LP) that is converted that is converted to the two ends of PM steel, and it can be calculated by:

$$\mathrm{Gm}\sigma = \mathrm{Gm}\sigma 1 + \mathrm{Gm}\sigma 2 + \mathrm{Gm}\sigma 3 \tag{6}$$

① $G_{m\sigma 1}$ is the LP between two axial end the surfaces of tile-shaped PM steel, and it can be calculated by:

$$G_{m\sigma 1} = 0.125\mu_0 h_m \tag{7}$$

where h_m is the width of tile-shaped PM steel, and $h_m = 2h_{m1}$.

② $G_{m\sigma 2}$ is the LP between the two sides of tile-shaped PM steel, its calculation formula is as follows:

$$G_{m\sigma 2} = \mu_0 \frac{l_{m1}}{\pi}\left[\left(\frac{a_2}{a_2 - a_1}\ln\frac{a_2}{a_1}\right) - 1\right] \tag{8}$$

where a_1 is the interelectrode distance of tile-shaped PM steel in the direction of the inside diameter, and, $a_1 = \frac{\theta_1\pi}{180}R_{r0}$, where θ_1 is the included angle of tile-shaped PM steel, R_{r0} is the radius of the rotor core, and a_2 is the interelectrode distance of tile-shaped PM steel in the direction of the external diameter; and $a_2 = \frac{\theta_1\pi}{180}(R_{r0} + b_{m1})$.

③ $G_{m\sigma 3}$ is the LP of the non-magnetic screw and can be calculated by:

$$G_{m\sigma 3} = \mu_{r2}\mu_0 \frac{\pi d_{ld}^2}{2l_{ld}} \tag{9}$$

where μ_{r2} is the relative magnetic permeability of stainless steel, and $\mu_{r2} = 1.3$; d_{ld} is the diameter of the non-magnetic screw; and l_{ld} is the effective length of the screw, $l_{ld} = b_{m1}$.

6) G_P is the permeance of pole boots, and it can be calculated by:

$$G_p = \mu_{r3}\mu_0 \frac{S_p}{b_p} \tag{10}$$

where μ_{r3} is the relative magnetic permeability of iron, and $\mu_{r3} = 2000$; S_P is the entire surface area of one pole boot, $S_P = S_{m1}$; and b_P is the thickness of pole boots.

7) G_{mp} is the LP between adjacent pole boots and can be calculated by:

$$G_{mp} = \mu_0 \frac{b_p}{\tau - h_p} l_p \tag{11}$$

where τ is the polar distance; h_P is the width of pole boots, $h_P = 2h_{m1;}$ and l_P is the axial length of pole boots, $l_P = l_{m1}$.

8) G_δ is the main air-gap permeance and can be calculated as follows:

$$G_\delta = \mu_0 \frac{S_\delta}{\delta} \tag{12}$$

$$\begin{cases} \Phi_m = \Phi_{m\sigma} + \Phi_{mp} + \Phi_{mc} + \Phi_u \\ F_{c1} = \Phi_m \dfrac{1}{G_{m1}} + \Phi_{m\sigma}\dfrac{1}{G_{m\sigma}} \\ \Phi_{m\sigma}\dfrac{1}{G_{m\sigma}} + F_{c1} + F_{c2} = (\Phi_m - \Phi_{m\sigma})\left(\dfrac{2}{G_{\delta 2}} + \dfrac{1}{G_{j3}} + \dfrac{2}{G_{\delta 3}} + \dfrac{1}{G_{m2}} + \dfrac{1}{G_{j2}} + \dfrac{1}{G_{m1}} + \dfrac{2}{G_{\delta 1}} + \dfrac{2}{G_p}\right) + \Phi_{mp}\dfrac{1}{G_{mp}} \\ \Phi_{mp}\dfrac{1}{G_{mp}} = (\Phi_m - \Phi_{m\sigma} - \Phi_{mp})\dfrac{2}{G_\delta} + \Phi_{mc}\dfrac{1}{G_{mc}} \\ \Phi_{mc}\dfrac{1}{G_{mc}} = \Phi_u\left(\dfrac{2}{G_t} + \dfrac{1}{G_{j1}}\right) + F_{ad} \end{cases} \tag{1}$$

where S_δ is the air-gap surface area between one magnetic pole of the PM rotor and stator, $S_\delta = S_{\mathrm{m1}}$, and δ is the air-gap length between the rotor and the stator.

9) $G_{\delta 1}$ is the additional air-gap permeance between the tile-shaped PM steel and the pole boots, it can be calculated by:

$$G_{\delta 1} = \mu_0 \frac{S_{\delta 1}}{\delta_{m1}} \tag{13}$$

where $S_{\delta 1}$ is the air-gap surface area between the tile-shaped PM steel and the pole boots, $S_{\delta 1} = S_{\mathrm{m1}}$, and δ_{m1} is the air-gap length between the tile-shaped PM steel and the pole boots.

10) $G_{\delta 2}$ is the additional air-gap permeance between the rotor core and the tile-shaped PM steel, and its calculation formula is as follows:

$$G_{\delta 2} = \mu_0 \frac{S_{\delta 2}}{\delta_{m2}} \tag{14}$$

where $S_{\delta 2}$ is the air-gap surface area between the rotor core and the tile-shaped PM steel, $S_{\delta 2} = S_{\mathrm{m1}}$, and δ_{m2} is the air-gap length between the rotor core and the tile-shaped PM steel.

11) $G_{\delta 3}$ is the additional air-gap permeance between the rotor core and the rectangle PM steel, and it can be calculated by:

$$G_{\delta 3} = \mu_0 \frac{S_{\delta 3}}{\delta_{m3}} \tag{15}$$

where $S_{\delta 3}$ is the air-gap surface area between the rotor core and the rectangle PM steel, $S_{\delta 3} = S_{\mathrm{m3}}$, and δ_{m3} is the air-gap length between the rotor core and the rectangle PM steel.

12) G_{mc} is the total LP between stator teeth and can be obtained by calculating the value of each part of the stator slot. The stator slot and stator leakage flux calculation segment diagram are shown in Figure 4, and G_{mc} is calculated as follows:

$$\mathrm{Gmc} = \mathrm{Gmc1} + \mathrm{Gmc2} + \mathrm{Gmc3} + \mathrm{Gmc4} \tag{16}$$

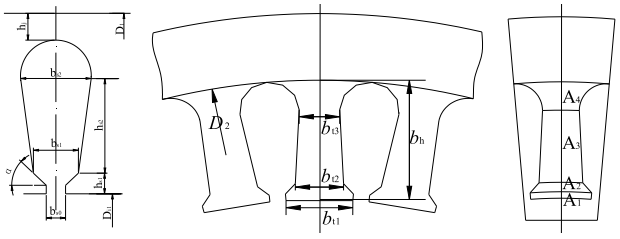

FIGURE 4. Schematic diagram of the stator slot and stator tooth of the generator.

① G_{mc1} is the LP of the rectangle part of the stator slot notch, and it can be calculated by:

$$G_{mc1} = \mu_0 L_m \frac{2h_{s1} - (b_{s1} - b_{s0})\, tg\alpha}{2b_{s0}} \tag{17}$$

where L_{m} is the thickness of the stator iron core; h_{s1} is the height of the stator slot wedge; b_{s1} is the width of the small end of the stator slot; b_{s0} is the width of the stator slot notch; and α is the angle between the slot wedge inclined plane and stator tooth.

② G_{mc2} is the LP of the first isosceles trapezoid portion of the stator slot, and it can be calculated by:

$$G_{mc2} = \mu_0 L_m \frac{(b_{s1} - b_{s0})\, tg\alpha}{b_{s1} + b_{s0}} \tag{18}$$

③ G_{mc3} is the LP of second isosceles trapezoid portion of the stator slot, and it can be calculated by:

$$G_{mc3} = \mu_0 L_m \frac{2h_{s2}}{b_{s2} + b_{s1}} \tag{19}$$

where h_{s2} is the trapezoid height of the stator slot, and b_{s2} is the width of the big end of the stator slot.

④ G_{mc4} is the LP of the semi-circular portion of the stator slot, and it can be calculated by:

$$G_{mc4} = \mu_0 L_m \frac{2}{\pi} \tag{20}$$

Therefore, the total LP between stator teeth is:

$$G_{mc} = \mu_0 L_m \left[\frac{2h_{s1} - (b_{s1} - b_{s0})tg\alpha}{2b_{s0}} + \frac{(b_{s1} - b_{s0})tg\alpha}{b_{s1} + b_{s0}} + \frac{2h_{s2}}{b_{s2} + b_{s1}} + \frac{2}{\pi} \right] \tag{21}$$

13) G_{t} is the total permeance of stator tooth, which can be obtained by dividing stator tooth to different parts according to the magnetic circuit and calculating the permeance of each part. The stator tooth can be divided into an approximate rectangle (A_1), two isosceles trapezoids (A_2 and A_3) and an irregular pattern (A_4), which is shown in the C diagram in Figure 4. The departments of A_1, A_2, A_3 and A_4 are connected in series, and the total permeance G_{t} can be calculated as:

$$\frac{1}{G_{\mathrm{t}}} = \frac{1}{G_{\mathrm{t1}}} + \frac{1}{G_{\mathrm{t2}}} + \frac{1}{G_{\mathrm{t3}}} + \frac{1}{G_{\mathrm{t4}}} \tag{22}$$

① G_{t1} is the permeance of part A_1, and it can be calculated by:

$$G_{t1} = \mu_{r4}\mu_0 \frac{S_{t1}}{b_{t1}} \tag{23}$$

where μ_{r4} is the relative magnetic permeability of silicon steel, and $\mu_{\mathrm{r4}} = 8000$; S_{t1} is the average cross sectional area of an approximate rectangle (part A_1), $S_{t1} = b_{t1}L_{\mathrm{m}}$; and b_{t1} is the stator tooth width, and, $b_{\mathrm{t1}} = \frac{\pi D_{\mathrm{i1}}}{36} - b_{\mathrm{s0}}$, where D_{i1} is the inner circle diameter of stator, and L_{m} is the length of the stator core.

② G_{t2} is the permeance of part A_2, and it can be calculated by:

$$G_{t2} = \mu_{r4}\mu_0 \frac{S_{t2}}{b_{t2}} \tag{24}$$

where S_{t2} is the average cross sectional area of the isosceles trapezoid (part A_2), $S_{t2} = \frac{1}{2}(b_{t1} + b_{t2})\, L_m$; b_{t2} is the width of the big end of the stator tooth, and $b_{\mathrm{t2}} = \frac{\pi\left(D_{\mathrm{i1}} + h_{\mathrm{s1}}\right)}{36} - b_{\mathrm{s1}}$.

③ G_{t3} is the permeance of part A_3, and it can be calculated by:

$$G_{t3} = \mu_{r4}\mu_0 \frac{S_{t3}}{b_{t3}} \tag{25}$$

where S_{t3} is the average cross sectional area of the isosceles trapezoid (part A_3), and $S_{t2} = \frac{1}{2}(b_{t1} + b_{t2}) L_m$, where b_{t3} is the width of the small end of the stator tooth, and

$$b_{t3} = \frac{\pi\left(D_{i1+h_{s1}} + h_{s2}\right)}{36} - b_{s2}.$$

③ G_{t4} is the permeance of part A_4, and it can be calculated by:

$$G_{t4} = \mu_{r4}\mu_0 \frac{S_{t4}}{b_{t4}} \tag{26}$$

where S_{t4} is the average cross sectional area of irregular graphics (part A_4), because part A_4 is approximately a isosceles trapezoid, $S_{t4} = \frac{1}{2}\left[b_{t3} + \frac{\pi(b_h + D_{i1})}{36}\right] L_m$, where b_{t4} is the radial average length of part A_4, and $b_{t4} = \frac{b_{s2}}{2}$.

14) G_{j1} is the stator yoke permeance and it can be calculated as follows:

$$G_{j1} = \mu_{r4}\mu_0 \frac{S_{j1}}{b_{j1}} \tag{27}$$

where S_{j1} is the average cross sectional area of the stator yoke, $S_{j1} = h_j L_m$, where b_{j1} is the tangential average length of the stator yoke. The section of the stator yoke is similar to a ring, so, $b_{j1} = \frac{\pi}{12}(D_1 + D_{i1} + b_h)$, where D_1 is the outer circle diameter of the stator.

15) G_{j2} is the permeance of rotor core from the tile-shaped PM steel to the rectangle PM steel, and it can be calculated by:

$$G_{j2} = \mu_{r4}\mu_0 \frac{S_{j2}}{b_{j2}} \tag{28}$$

where S_{j2} is the average cross sectional area of the rotor core from the tile-shaped PM steel to the rectangle PM steel, $S_{j2} = \theta \frac{\pi}{180}\left(R_{r0} - \frac{1}{2}t_3\right) l_m$, where θ is the angle between magnetism isolating air-gap II and the abscissa of the axis center, t_3 is the distance from the rectangle PM steel to the edge of the rotor core, and l_m is the thickness of the rotor core, $l_m = l_{m1;}b_{j2}$ is the radial average length of the rotor core from the tile-shaped PM steel to the rectangle PM steel, and $b_{j2} = \left[t_3 + \left(R_{r0} - \frac{h_{m1}}{\sin\theta}\right)\right]$. The specific size of the PM rotor is shown in Figure 2.

16) G_{j3} is the permeance of the rotor core from rectangle PM steel to tile-shaped PM steel, and it can be calculated by:

$$G_{j3} = \mu_{r4}\mu_0 \frac{S_{j3}}{b_{j3}} \tag{29}$$

where S_{j3} is the average cross sectional area of the rotor core from rectangle PM steel to tile-shaped PM steel, $S_{j3} = \left[\frac{\pi h_{m1}}{4\tan\theta} - (2h_{m1} - h_{m2})\right] l_m$. b_{j3} is the radial average length of the rotor core from the rectangle PM steel to tile-shaped PM steel, $b_{j3} = 2\left[R_{r0} - (R_z + t_1 + t_2)\right] - t_3$, where R_z is the radius of rotor shaft, t_1 is the thickness of the magnetic isolation bushing, and t_2 is length of the magnetic isolation bushing bulge.

The leakage coefficient of the double-radial PM generator can be obtained using the above settlement formula.

$$\sigma_0 = \frac{\Phi_m}{\Phi_u} \tag{30}$$

Because the leakage coefficient of the double-radial PM rotor is large and the utilization of PM steel is low, it is necessary to take effective measures to reduce magnetic leakage [23]. To reduce the magnetic leakage between pole boots, we can use a magnetic separation material to fill the gap between the pole boots. In order to avoid the magnetic leakage between two poles of PM steel, we can add magnetic isolation bushing on the shaft [25].

B. MAGNETIC FIELD SIMULATION ANALYSIS

The magnetic field mathematical model is established according to Maxwell equations [26], [27], as follows:

$$\begin{cases} \oint_l H \cdot dl = \int_S (J + \dfrac{\partial D}{\partial t}) \cdot dS \\ \oint_l E \cdot dl = -\int_S \dfrac{\partial B}{\partial t} \cdot dS \\ \oint_S B \cdot dS = 0 \\ \oint_S D \cdot dS = \int_V \rho \cdot dV \end{cases} \tag{31}$$

where H is the magnetic field intensity, and its unit is A/m; J is the current density, and its unit is A/m2; E is the electric field intensity, and its unit is V/m; B is the magnetic induction, and its unit is T; D is the electric displacement vector, and its unit is C/m2; and ρ is the charge density, and its unit is C/m3. And the relationships among the field quantities of the above model are: $D = \varepsilon E$, $B = \mu H$, $J = \sigma E$, where ε is the dielectric coefficient, and its unit is F/m; μ is the permeability, and its unit is H/m; and σ is the electronic conductivity, and its unit is S/m.

By meshing the model, setting the magnetization direction, applying a load and setting the boundary conditions, we establish the finite-element model of the double-radial PM generator as shown in Figure 5. By analyzing the generator

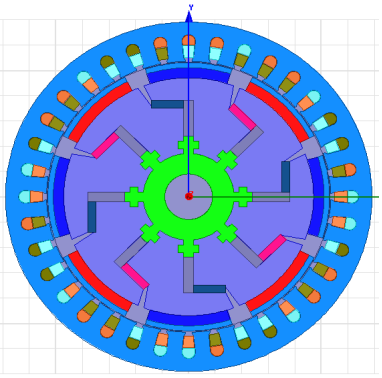

FIGURE 5. 2D model of the double-radial PM generator.

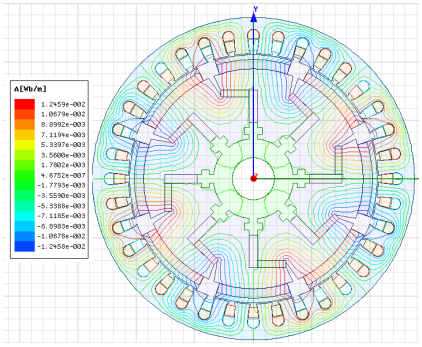

FIGURE 6. Flux distribution diagram.

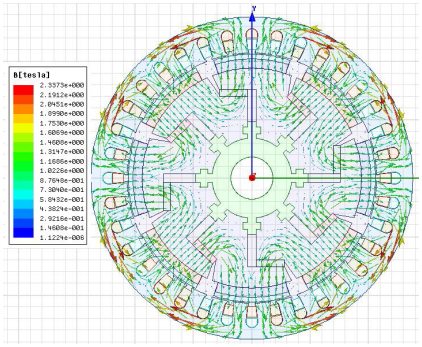

FIGURE 7. Magnetic flux density vector diagram.

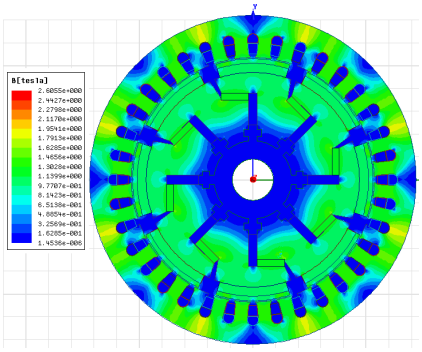

FIGURE 8. Modulus value of the magnetic flux density.

model, we obtain the flux distribution, magnetic flux density vector diagram and modulus value of the magnetic flux density, which are shown in Figure 6 to Figure8.

In Figure 6, on the same magnetic pole, the magnetic flux is provided by two adjacent tile-shaped PM steels and one rectangular PM steel, and the distribution of the magnetic field is uniform. The vector diagram of the magnetic flux density shows that the direction of the simulated magnetic field is identical to that of the designed magnetic field. As shown in Figure 8, the magnetic flux density of the air-gap is 1.5 T, which has not reached the saturation flux density of silicon and satisfied the design requirement [28]–[30].

III. PERFORMANCE TEST

To obtain the optimal parameters that match with the entire machine, the main parameters, which include the thickness of PM steel in the magnetization direction, length of PM steel, number of pole-pairs, the thickness of spacer bush, turns of each armature winding, cross sectional area of armature winding conductor, etc., are optimized in performance tests.

1) The thickness of PM steel in the magnetization direction

When the thicknesses of PM steel in magnetization direction is 2.0 mm, 2.5 mm, 3.0 mm, and 3.5 mm, the output voltages are tested and shown in Figure 9.

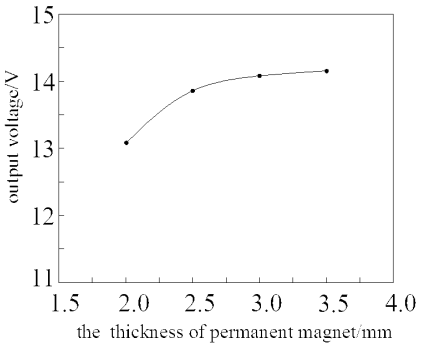

FIGURE 9. The output voltage with different thickness values of PM steel in the magnetization direction.

In Figure 9, when the thickness of PM steel in the magnetization direction is small, the output voltage increases when the thickness increases. When the thickness reaches a certain value, the change of output voltage is not obvious with the increase in thickness. This particular thickness can become the optimal thickness of PM steel in the magnetization direction and is 3 mm.

2) Length of PM steel

When the length of PM steel is 20 mm, 25 mm, 30 mm, and 35 mm, the output voltages are tested and shown in Figure 10.

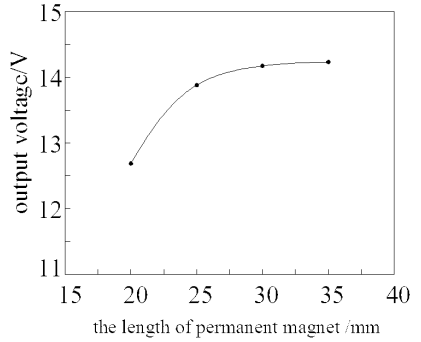

FIGURE 10. The output voltage with different lengths of PM steel.

In Figure 10, when the length of PM steel is small, the output voltage quickly increases with the increase in length. When the PM steel length reaches a certain value, the output voltage slowly increases with the increase in length. This particular length can become the optimal length of PM steel and is 32 mm.

3) Number of pole-pairs

When the number of pole-pairs is 5, 6, 7, and 8, the output voltages of generator are tested and illustrated in Figure 11.

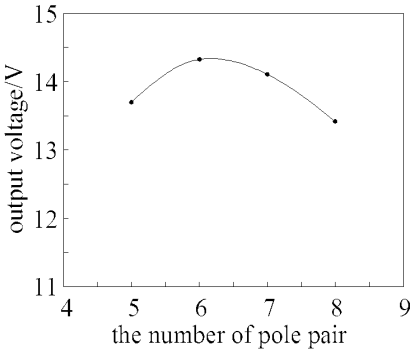

FIGURE 11. The output voltage with different pole-pairs.

In Figure 11, when the number of pole-pairs is small, the frequency and output voltage are low. Hence, the output voltage quickly increases when the number of pole-pairs increases. When the numbers of pole-pairs reach a certain value, the output voltage is maximal. Then, with the increase of the number of pole-pairs, the output voltage decreases because of the increase of internal reactance, therefore, more pole-pairs are not necessarily better. The overall performance and the use of PM steel magnetic properties should be considered. In this paper, the better number of pole-pairs is 6.

4) The thickness spacer bush

When the thickness of the spacer bush is 2 mm, 3 mm, 4 mm, and 5 mm, the output voltage is tested and shown in Figure 12.

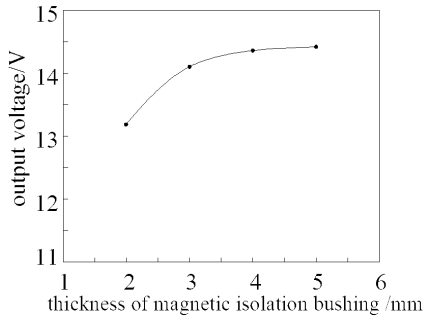

FIGURE 12. The output voltage with different spacer bush thickness.

In Figure 12, when the thickness of the spacer bush is small, the output voltage is low because of magnetic leakage. It quickly increases with the increase of spacer bush thickness, but the increase rate decreases when the thickness reaches a certain value. Therefore, the spacer bush thickness should be appropriate, if the thickness is too small, the magnetic leakage will be very large. And if the thickness is too large, the use space of PM steel will be reduced. In this paper, the thickness of the spacer bush is 4 mm.

5) Turns of armature winding

When the rotor parameters of the generator are decided, the turns of each armature winding are 5 turns, 6 turns, 7 turns, and 8 turns, respectively. The output voltage are tested and shown in Figure 13.

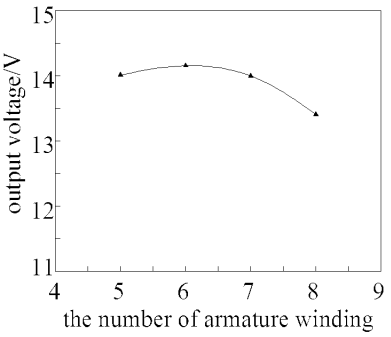

FIGURE 13. The output voltage cure with various numbers of per pole armature winding turns.

In Figure 13, the output voltage increases when the armature winding turns are small and decreases when the turns reach a certain value because of the increase in internal reactance. In this paper, the number of armature winding turns is 6.

6) Cross sectional area of the armature winding conductor

When the parameters of the generator rotor and number of armature winding turns are decided, the cross sectional areas of the armature winding conductor are 4.4 mm^2, 4.6 mm^2, 4.8 mm^2, and 5 mm^2, respectively. The output voltage curve with different cross sectional areas is illustrated in Figure 14.

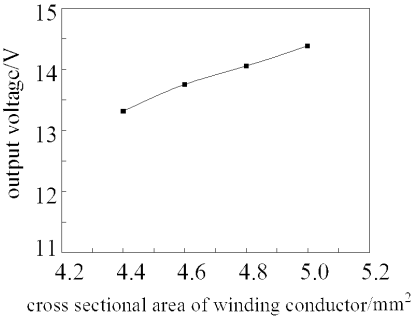

FIGURE 14. The output voltage with different cross sectional areas of the armature winding conductor.

As seen from Figure 14, the larger the cross sectional area of armature winding, the higher the output voltage. However, if the cross sectional area is too large, the generator volume will increase, and the cost will be very high. In this paper, the cross sectional area of armature winding conductor is 4.8 mm^2.

Through the parameter optimization analysis, Nd-Fe-B is used as the PM material, and its remnant magnetic induction (Br) is 1.27 T, the coercivity (H_c) is 915 kA/m, and the maximum energy product ($(BH)_{max}$) is 295 kJ/m^3 [31], [32]. The thickness of PM steel in the magnetization direction is 3 mm, the length of PM steel is 32 mm, the number of pole-pairs is 6, the thickness of spacer bush is 4 mm, the number of armature winding turns is 6, the cross sectional area of the

armature winding conductor is 4.8 mm^2, The generator rated voltage is 14 V, the rated power is 2000 W, and the rated speed is 4000 r/min. The newly developed double-radial rare-earth PM voltage-stabilizing generation device is tested from low speed to high speed in the generator comprehensive performance test-bad, and the test results are shown in Table 1.

TABLE 1. Generator output voltage with various rotary speeds and load powers.

Speed r/min	Load power kW	Prototype voltage V
2000	1.9	13.62
	2.0	13.31
	2.1	13.13
4000	1.9	14.31
	2.0	14.23
	2.1	14.15
4800	1.9	14.28
	2.0	14.23
	2.1	14.14

Table 1 shows that the performance indicators can satisfy the design requirement. When the generator speed varies from 2000 r/min to 4800 r/min and the load power varies from 1.9 kW to 2.1 kW, the output voltages remain steady at 13.13 $\sim$ 14.31 V, which shows that the designed generator has good regulator performance.

IV. CONCLUSIONS

In this paper, the TEMCM is adapted to establish the EMCM of the double-radial rare-earth PM generator, the influence factors of the leakage coefficient are analyzed, and magnetic isolation measures are taken to reduce magnetic leakage and improve the generator efficiency.

The major parameters of the designed generator are experimentally analyzed, and the optimal matching parameters are obtained. As a result, a double-radial rare-earth PM generator is developed and which has the advantages of low power consumption, low failure rate, high efficiency and high power density.

To validate the performance of the developed generator, performance tests are performed with various rotary speeds and load power. The results show that when the speed varies from 2000 r/min to 4800 r/min and the load power varies from 1900 W to 2100 W, the output voltage remains steady at 13.13 $\sim$ 14.31 V, which indicates that the designed generator has a good regulator performance.

REFERENCES

[1] M. Koichi, "Development trend of the permanent magnet synchronous motor for rail vehicle traction," *J. Inst. Elect. Eng. Jpn.*, vol. 126, no. 11, pp. 729–731, 2006.

[2] F. Zhang, J. Xu, G. Jia, and S. Jin, "Electromagnetic design and dynamic performance study of electrically excited brushless synchronous motor," in *Proc. IEEE Int. Conf. Elect. Mach. Syst. (ICEMS)*, Oct. 2013, pp. 699–702.

[3] M. Franko, J. Kuchta, and J. Buday, "Development and performance investigation of permanent magnet synchronous traction motor," in *Proc. IEEE Int. Symp. Power Electron., Elect. Drives, Autom. Motion (SPEEDAM)*, Jun. 2012, pp. 70–74.

[4] X.-Y. Zhang and Q.-L. Zeng, "Development on rare-earth permanent-magnet generator with vacuum pump for vehicle," *Mach. Des. Manuf.*, vol. 7, pp. 134–136, Jul. 2009.

[5] H. Q. Xu, "Research on the steady voltage of permanent-magnet generator with pressure roller on the vehicle," *Appl. Mech. Mater.*, vols. 291–294, pp. 2507–2512, Feb. 2013.

[6] S. Javadi and M. Mirsalim, "Design and analysis of 42-V coreless axial-flux permanent-magnet generators for automotive applications," *IEEE Trans. Magn.*, vol. 46, no. 4, pp. 1015–1023, Apr. 2010.

[7] H. Zhang, X. Zhang, C. Gerada, M. Galea, D. Gerada, and J. Li, "Armature design of an ultra-high speed PM generator," in *Proc. IEEE Conf. Electromagn. Field Comput. (CEFC)*, vol. 11. Nov. 2016, p. 1.

[8] K. Nishida, T. Ahmed, and M. Nakaoka, "Advanced active power filter controlled permanent-magnet synchronous generator for automotive applications," in *Proc. IEEE Power Electron. Spec. Conf.*, Jun. 2007, pp. 1508–1514.

[9] T.-F. Chan, W. Wang, and L.-L. Lai, "Permanent-magnet synchronous generator supplying an isolated load," *IEEE Trans. Magn.*, vol. 46, no. 8, pp. 3353–3356, Aug. 2010.

[10] W. Cheng, Y. Sun, Y. Tian, and Y. Lie, "An analytical model for performance estimation of high speed PM generator," in *Proc. IEEE Conf. Expo Transp. Electrific. Asia–Pacific*, Aug. 2014, pp. 1–6.

[11] A. A. Qazalbash, S. M. Sharkh, N. T. Irenji, R. G. Wills, and M. A. Abusara, "Rotor eddy loss in high-speed permanent magnet synchronous generators," *IET Electr. Power Appl.*, vol. 9, no. 5, pp. 370–376, May 2015.

[12] G.-H. Jang, M.-M. Koo, S.-W. Seo, K. Hong, and J.-Y. Choi, "Eddy current loss in double-sided cored slotless type permanent magnet linear synchronous generator using analytical method," *AIP Adv.*, vol. 7, no. 5, p. 056610, 2017.

[13] X. Zhang, W. Li, H. Qiu, and S. Cheng, "Calculation of electromagnetic field and temperature field in super high speed permanent magnet generator with composite structures," *Proc. Chin. Soc. Elect. Eng.*, vol. 31, no. 30, pp. 85–92, 2011.

[14] J.-Q. Wang, F.-X. Wang, and X.-G. Kong, "Design and analysis of electromagnetic properties for high speed PM generator," *Proc. Chin. Soc. Elect. Eng.*, vol. 28, no. 20, pp. 105–110, 2008.

[15] Y. Feng *et al.*, "Date-driven accurate design of variable blank holder force in sheet forming under interval uncertainty using sequential approximate multi-objective optimization," *Future Generat. Comput. Syst.*, 2017. [Online]. Available: http://dx.doi.org/10.1016/j.future.2017.02.048

[16] Y. Gao, Y. Feng, Z. Zhang, and J. Tan, "An optimal dynamic interval preventive maintenance scheduling for series systems," *Rel. Eng. Syst. Saf.*, vol. 142, pp. 19–30, Oct. 2015.

[17] K. Wang, H. Li, Y. Feng, and G. Tian, "Big data analytics for system stability evaluation strategy in the energy Internet," *IEEE Trans. Ind. Informat.*, vol. 13, no. 4, pp. 1969–1978, Aug. 2017.

[18] J. Wang, M. West, D. Howe, H. Z.-D. La Parra, and W. M. Arshad, "Design and experimental verification of a linear permanent magnet generator for a free-piston energy converter," *IEEE Trans. Energy Convers.*, vol. 22, no. 2, pp. 299–306, Jun. 2007.

[19] S. M. Hosseini, M. Agha-Mirsalim, and M. Mirzaei, "Design, prototyping, and analysis of a low cost axial-flux coreless permanent-magnet generator," *IEEE Trans. Magn.*, vol. 44, no. 1, pp. 75–80, Jan. 2008.

[20] S. Zhou, H. Yu, M. Hu, C. Jiang, and L. Huang, "Nonlinear equivalent magnetic circuit analysis for linear flux-switching permanent magnet machines," *IEEE Trans. Magn.*, vol. 48, no. 2, pp. 883–886, Feb. 2012.

[21] Y.-C. Wu and B.-S. Jian, "Magnetic field analysis of a coaxial magnetic gear mechanism by two-dimensional equivalent magnetic circuit network method and finite-element method," *Appl. Math. Model.*, vol. 39, no. 19, pp. 5746–5758 2014.

[22] S.-H. Lee, S.-O. Kwon, J.-J. Lee, and J.-P. Hong, "Characteristic analysis of claw-pole machine using improved equivalent magnetic circuit," *IEEE Trans. Magn.*, vol. 45, no. 10, pp. 4570–4573, Oct. 2009.

[23] S. Javadi and M. Mirsalim, "A coreless axial-flux permanent-magnet generator for automotive applications," *IEEE Trans. Magn.*, vol. 44, no. 12, pp. 4591–4598, Dec. 2008.

[24] H. Gör and E. Kurt, "Preliminary studies of a new permanent magnet generator (PMG) with the axial and radial flux morphology," *Int. J. Hydrogen Energy*, vol. 41, no. 17, pp. 7005–7018, 2016.

[25] P. Jin, S. Fang, H. Lin, Z. Q. Zhu, Y. Huang, and X. Wang, "Analytical magnetic field analysis and prediction of cogging force and torque of a linear and rotary permanent magnet actuator," *IEEE Trans. Magn.*, vol. 47, no. 10, pp. 3004–3007, Oct. 2011.

[26] K. Boughrara, R. Ibtiouen, D. Žarko, O. Touhami, and A. Rezzoug, "Magnetic field analysis of external rotor permanent-magnet synchronous motors using conformal mapping," *IEEE Trans. Magn.*, vol. 46, no. 9, pp. 3684–3693, Sep. 2010.
[27] S. Zhou, M. H. Li, and Y. Zhou, "Modeling and simulation of six-phases trapezoidal permanent magnet generator with rectifying load," *Small Special Elect. Mach.*, vol. 44, no. 1, pp. 7–11, 2016.
[28] Q. J. Ze, D. Liang, P. Kou, and Y. Yu, "Improvement of power generation performance in a doubly salient permanent magnet generator with a capacitive energy recovery converter," *IET Electr. Power Appl.*, vol. 11, no. 1, pp. 108–120, 2017.
[29] X. Zhang *et al.*, "Nd-Fe-B permanent magnet generator and voltage stabilizing control technology for vehicles," *Adv. Mech. Eng.*, vol. 8, no. 9, pp. 1–11, 2016.
[30] G. Bai, R. W. Gao, Y. Sun, G. B. Han, and B. Wang, "Study of high-coercivity sintered NdFeB magnets," *J. Magn. Magn. Mater.*, vol. 308, no. 1, pp. 20–23, 2007.
[31] S. Morimoto, "Trend of permanent magnet synchronous machines," *IEEJ Trans. Elect. Electron. Eng.*, vol. 2, no. 2, pp. 101–108, Mar. 2007.

XUEYI ZHANG received the M.S. degree in mechanical manufacturing automation from Guangxi University, Nanning, China, in 1990, and the Ph.D. degree in mechanical and electronic engineering from the Shandong University of Science and Technology University, Qindao, China, in 2011. He is currently with the School of Transportation and Vehicle Engineering, Shandong University of Technology, where he is involved in the research and development of vehicle's motor and electric vehicles. He is a National Candidate of Millions of Talents. He received the Second Award of National Technical Invention and six items the Second Prizes at provincial and ministerial level. He has 14 authorized patents. He has released 112 papers and published five monographs. He is receiving the State Department Special Allowance.

QINJUN DU received the M.S. degree in agricultural electrical and automation from China Agricultural University, Beijing, China, in 2003, and the Ph.D. degree in bionic bechnology from the Beijing Institute of Technology, Beijing, in 2007. He is currently with the School of Electrical and Electronic Engineering, Shandong University of Technology, where he is involved in the research and development of electronic and electrical technology for vehicle. He has released 43 papers. He received the Young Experts with outstanding contributions in Shandong Province. He also received the Second Award of National Technical Invention and three items the Second Prize at provincial and ministerial level.

SHILUN MA received the M.E. degree in agricultural mechanization from Gansu Agricultural University, Lanzhou, Gansu, China, in 2015.

He is currently pursuing the Ph.D. degree with the Transportation and Vehicle Engineering School, Shandong University of Technology, Shandong, China. His research interests focuses on vehicle engineering, automotive electronics, and design and manufacture of motor and new energy electric vehicle technology.

HUIHUI GENG received the B.S. degree in communications and transportation engineering from the Shandong University of Technology, Zibo, China, in 2015, where she is currently pursuing the M.S. degree with the Transportation and Vehicle Engineering School. Her research interests focuses on vehicle engineering, automotive electronics, and design and manufacture of motor and new energy electric vehicle technology.

WENJING HU received the B.S. and M.S. degrees in vehicle engineering from the Shandong University of Technology, Zibo, China, in 2015 and 2017, respectively, where she is currently pursuing the Ph.D. degree with the Transportation and Vehicle Engineering School. Her research interests focuses on vehicle engineering, automotive electronics, and design and manufacture of motor and new energy electric vehicle technology.

ZHIWU LI (M'06–SM'07–F'16) received the B.S. degree in mechanical engineering, the M.S. degree in automatic control, and the Ph.D. degree in manufacturing engineering from Xidian University, Xi'an, China, in 1989, 1992, and 1995, respectively. He joined Xidian University in 1992. Over the past decade, he was a Visiting Professor with the University of Toronto, the Technion—Israel Institute of Technology, the Martin Luther University of Halle-Wittenberg, the Conservatoire National des Arts et Métiers (Cnam), Meliksah Universitesi, King Saud University, and the University of Cagliari. He is currently with the Institute of Systems Engineering, Macau University of Science and Technology, Macau. His current research interests include Petri net theory and application, supervisory control of discrete event systems, work flow modeling and analysis, system reconguration, game theory, and data and process mining.

Dr. Li was a member of the IFAC Technical Committee on Discrete Event and Hybrid Systems from 2011 to 2014. He is a member of the Discrete Event Systems Technical Committee of the IEEE Systems, Man, and Cybernetics Society He is a recipient of an the Alexander von Humboldt Research Grant, the Alexander von Humboldt Foundation, Germany, and a Research in Paris, France. He is the Founding Chair of the Xi'an Chapter of the IEEE Systems, Man, and Cybernetics Society. He serves as a Frequent Reviewer for over 60 international journals including *Automatica* and a number of the IEEE TRANSACTIONS as well as many international conferences. He is listed in Marquis Who's Who in the world, 27th Edition, in 2010.

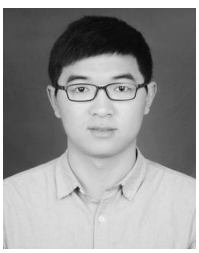

GUOQIANG LIU received the B.S. degree in vehicle engineering from Shandong Jiaotong University, Jinan, China, in 2016.

He is currently pursuing the M.S. degree with the Transportation and Vehicle Engineering School, Shandong University of Technology, Zibo, China. His research interests focuses on vehicle engineering, automotive electronics, and design and manufacture of motor and new energy electric vehicle technology.